Dispersive instability and its minimization in time-domain computation of steady-state responses of cochlear models

Jack Xin[a)]
Department of Mathematics and ICES, University of Texas at Austin, Austin, Texas 78712

(Received 2 September 2003; revised 3 February 2004; accepted 18 February 2004)

Dispersive instability appears in time-domain solutions of classical cochlear models. In this letter, a derivation of optimal initial data is presented to minimize the effect of instability. A second-order accurate implicit boundary integral method is introduced. Numerical solutions of two-dimensional models show that the optimal initial conditions work successfully in time-domain steady-state computations for both the zero Neumann and zero Dirichlet fluid pressure boundary conditions at the helicotrema. © *2004 Acoustical Society of America.* [DOI: 10.1121/1.1699393]

PACS numbers: 43.64.Kc [JBS] Pages: 2173–2177

I. INTRODUCTION

Time-domain computation of cochlear models is necessary for computing basilar-membrane (BM) responses in the presence of nonlinearities.[1–4] However, time-domain solutions are prone to dispersive instability[4] even at the linear level. In Sec. II, illustrative numerical examples are given on such an instability arising in time-domain solutions of classical linear cochlear models, where frequency-domain solutions are perfectly fine.[5]

It is useful to investigate how to do away with the instability and capture steady states dynamically as fast in time as possible. The objective here is to come up with a robust and effective approach without modifying models or specializing model parameters. Though the dispersiveness of model equations is the source of the problem, the cure lies in choosing a class of initial data so that the instability can be minimized and steady-state responses effectively computed.

In Sec. III, precise conditions of such optimal initial data are derived for the two-dimensional model under zero Neumann fluid pressure boundary condition at the helicotrema. In Sec. IV, an associated second-order accurate implicit boundary integral method is presented and analyzed. Numerical results show that the optimal initial data work effectively for both zero Neumann and zero Dirichlet pressure boundary conditions. Conclusions are given in Sec. V.

II. DISPERSIVE INSTABILITY

Classical one-dimensional transmission line model reads[6]

$$p_{xx} - N u_{tt} = 0, \quad x \in (0,L), \tag{2.1}$$

$$p = m u_{tt} + r u_t + s(x) u, \tag{2.2}$$

where p is the fluid pressure difference across the basilar membrane (BM), u the BM displacement, L the longitudinal length of BM with stapes located at $x=0$, and helicotrema at $x=L$; N a constant equal to fluid density times the ratio of BM width and scala cross section; m,r,s are the mass, damping, and stiffness of BM per unit area, respectively, with m and r being positive constants, and s a known function of x. The scala fluid motion obeys incompressible Stokes system with constant density.

Equations (2.1)–(2.2) are evolved in time with the boundary and initial data[2]

$$p_x(0,t) = p_{\text{in}}(t), \quad p(L,t) = 0, \tag{2.3}$$

$$u(x,0) = 0, \quad u_t(x,0) = 0, \tag{2.4}$$

where p_{in} is proportional to stapes acceleration driven by input signal.

The classical two-dimensional model replaces (2.1) by the Laplace equation on p thanks to the incompressibility of fluids[3,5]

$$p_{xx} + p_{zz} = 0, \quad (x,z) \in (0,L) \times (0,H), \tag{2.5}$$

subject to boundary conditions

$$p_x|_{x=0} = -2\rho\xi(t), \quad p|_{x=L} = 0, \tag{2.6}$$

$$p_z|_{z=0} = 2\rho u_{tt}, \quad p_z|_{z=H} = 0, \tag{2.7}$$

where H is the vertical height, ρ the fluid volume density, $\xi(t)$ the stapes acceleration. The initial condition (2.4) remains the same.[3]

The time-dependent systems above are known to be dispersive. If one ignores the boundary conditions at $x=0, L$, real dispersion relation is obtained in closed form when setting $r=0$, s to a positive constant, and looking for plane waves. A dispersive wave property is that spatial long waves move faster than short waves.[4]

For single-frequency input, $\sin(2\pi f t + \varphi)$, the time-dependent solutions lock onto the input frequency in time and eventually develop a spatial profile. It is generally expected that the steady state is a time harmonic solution, or the imaginary part of the complex solution $\mathbf{A}(x,z;f)\exp\{i(2\pi f t + \varphi)\}$, known as the frequency-domain solution.

However in numerical computations, time-domain solutions $u(x,t)$ contain additional dispersive waves which may outgrow the desired response.[4] As an illustration, in Fig. 1, we show the BM displacement $u(x, t = 20\ \text{ms})$, when the input is $\sin(2\pi f t)$, $f = 3$ kHz, computed by a second-order accurate implicit finite difference method[4] of the one-

[a)]Electronic mail: jxin@math.utexas.edu.

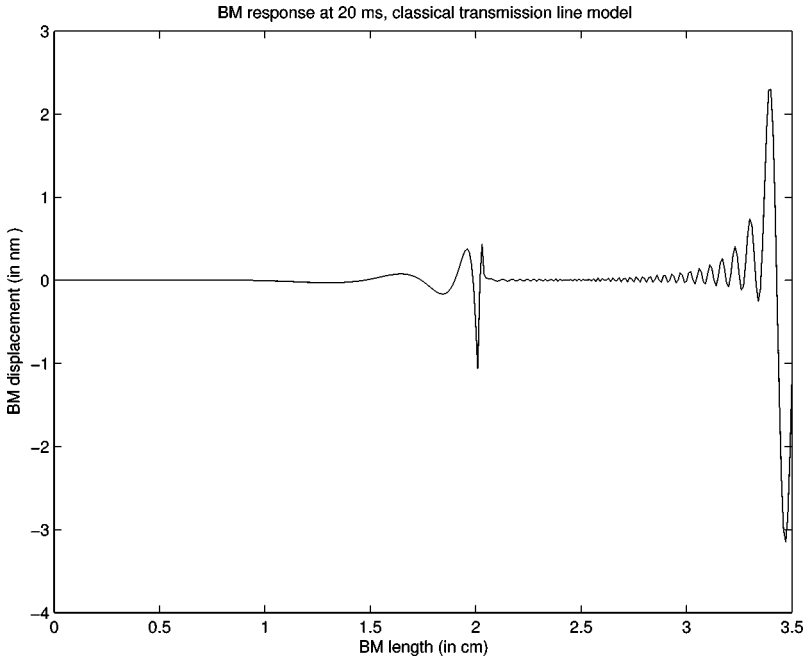

FIG. 1. BM displacement (in nm) at 20 ms with a sinusoidal input of 40 dB (SPL) and 3 kHz, computed by an implicit second-order finite difference method from the classical transmission line model (2.1)–(2.4). Mass density $m=0.05\ \mathrm{g/cm^2}$, damping constant $r=100\ \mathrm{dyn}\cdot\mathrm{s/cm^3}$, stiffness $s(x)$ as in (4.7). Midear factor is included. Steady state has formed to the left of the characteristic location (about 2 cm), yet to the right of it, dispersive instability is developed and persists afterward.

dimensional transmission line model with standard choice of coefficients. The dispersive waves are developed in the middle of the domain. They eventually travel to $x=L$ and remain there at later time. Figure 2 is a computed BM displacement at 10 ms from the two-dimensional model, using a second-order accurate implicit boundary integral method. The solution has reached steady state, yet the dispersive tail wave stays. The phenomenon is persistent under grid refinement, indicating that it is intrinsic to analytical solutions. Alternative numerical methods also reveal the same instability.

The key idea for developing a robust method to compute steady states in the time domain is to select suitable initial data different from the conventional data in (2.4) so as to minimize the growth of dispersive waves in the wake of steady states. Such optimal initial data shall depend on the input signal.

III. OPTIMAL INITIAL DATA

It is not obvious at all how to choose initial data in the systems (2.1)–(2.7) better than the natural all-zero data. Let us instead consider system (2.5)–(2.7), with the Dirichlet boundary condition $p|_{x=L}=0$ replaced by the zero Neumann boundary condition $p_x|_{x=L}=0$, or a rigid wall condition. At least for frequency-domain solutions, the resulting change is known to be insignificant; see the discussions in Neely[5] and references therein. However, there is a major difference in

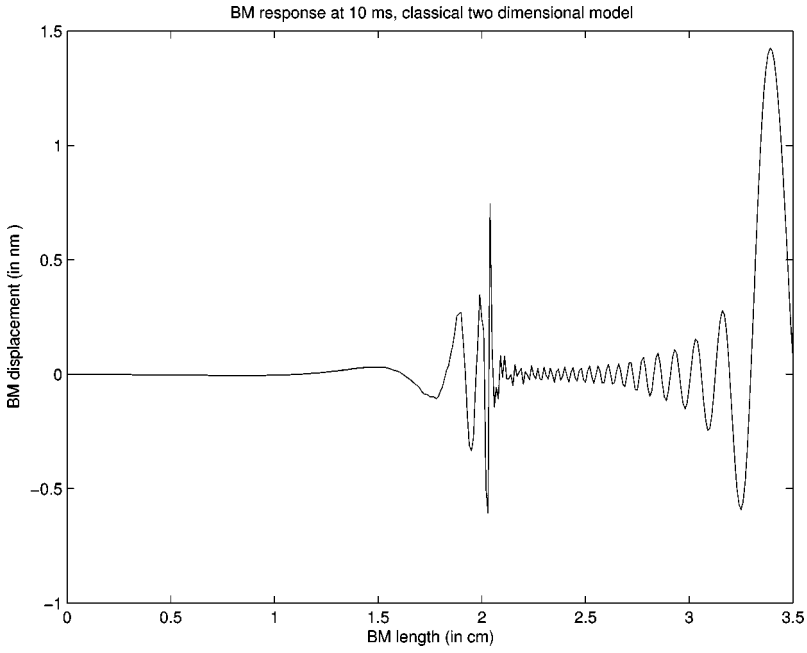

FIG. 2. BM displacement (in nm) at 10 ms with a sinusoidal input of 40 dB (SPL) and 3 kHz, computed by an implicit boundary integral method from the classical two-dimensional cochlear model (2.5)–(2.7). Model and numerical parameters are as in Sec. IV. Midear factor is included. Steady state has formed to the left of the characteristic location (about 2 cm), yet to the right of it, dispersive instability is developed and persists afterward.

mathematical formulation. A solvability condition must be imposed on the boundary data for the Neumann Laplacian, as a consequence of Green's theorem. It is

$$\int_0^L u_{tt}(x,t)dx = \xi(t)H, \tag{3.1}$$

which is preserved in time provided Eq. (2.2) is constrained as

$$p(x,0,t)+\lambda(t) = mu_{tt}+ru_t+s(x)u, \tag{3.2}$$

where $\lambda(t)$ is a time-dependent Lagrange multiplier so that (3.1) holds. It is clear that

$$\lambda(t) = -\frac{1}{L}\int_0^L [p(x,0,t)-ru_t-s(x)u]dx+\frac{m}{L}\xi(t)H. \tag{3.3}$$

The role of $\lambda(t)$ is to ensure that the evolution of u is consistent with the solvability condition (3.1) for all time. With this formulation, a time-domain method can be devised. Before we do that, let us extract some information about u from Eq. (3.1).

Integrating (3.1) in time twice, we find

$$\int_0^L u_t(x,t)dx = \alpha_1 + H\int_0^t \xi(\tau)d\tau, \tag{3.4}$$

and

$$\int_0^L u(x,t)dx = \alpha_2+\alpha_1 t + H\int_0^t dt'\int_0^{t'}\xi(\tau)d\tau, \tag{3.5}$$

where

$$\alpha_1 = \int_0^L u_t(x,0)dx, \tag{3.6}$$

$$\alpha_2 = \int_0^L u(x,0)dx. \tag{3.7}$$

For a general single-tone signal, $\xi(t)=A\sin(\omega t+\varphi)$, $\omega = 2\pi f$. The right-hand side of (3.5) is integrated exactly to give

$$\int_0^L u(x,t)dx = t(AH\omega^{-1}\cos\varphi+\alpha_1)+AH\omega^{-2} \times(\sin\varphi-\sin(\omega t+\varphi))+\alpha_2. \tag{3.8}$$

There is linear growth of $\int_0^L u(x,t)dx$ or instability unless

$$\alpha_1 = -AH\omega^{-1}\cos\varphi. \tag{3.9}$$

Interestingly, unless $\cos\varphi=0$, α_1 *should not equal zero*! This partially explains why instability is generic when computing the seemingly perfect system (2.1)–(2.7), assuming (and we shall see this is supported by numerics later) that the zero Neumann boundary condition at $x=L$ does little to the instability which arises in the interior of the computational domain.

Next, we choose α_2 as

$$\alpha_2 = -AH\omega^{-2}\sin\varphi, \tag{3.10}$$

so that

$$\int_0^L u(x,t)dx = -AH\omega^{-2}\sin(\omega t+\varphi), \tag{3.11}$$

has mean zero over $[0,T]$, where T equals the period f^{-1}.

Such a choice of α_2 also minimizes the L^2 norm square of $\int_0^L u(x,t)dx$ in the time interval $[0,T]$. In fact, it is easy to check that (3.11) is satisfied exactly by the time harmonic steady-state solution. For general signals, the optimality conditions on α_1 and α_2 can be derived by minimizing

$$\int_0^T\left[\alpha_2+\alpha_1 t+H\int_0^t dt'\int_0^{t'}\xi(\tau)d\tau\right]^2 dt,$$

over a large enough number T. Equivalently, one could do it frequency by frequency based on a spectral representation of the signal.

IV. NUMERICAL METHOD AND RESULTS

Let us consider the general single-tone input, and choose initial data as

$$u(x,0)=\alpha_2 g(x) \quad u_t=\alpha_1 g(x), \tag{4.1}$$

where $g(x)\in C^2([0,L])$, $g'(0)=g'(L)=0$, $\int_0^L g(x)dx=1$; and α_1, α_2 as in (3.9)–(3.10) so that (3.11) holds as a constraint for all time.

We shall compute with a boundary integral method by writing the pressure as a functional of u_{tt}, then reducing the problem to an integral-differential equation of u, and performing discretization. This is similar to the integral equation method in earlier works[1,3] except for the constraint (3.11). Inverting the Neumann Laplacian to solve for the pressure with the help of separation of variables, we obtain

$$\begin{aligned} p(x,0,t) &= \frac{\rho\xi(t)}{L}((x-L^2)-H^2) \\ &\quad -4\rho\sum_{k=1}^{\infty}\frac{\int_0^L u_{tt}\cos(k\pi x/L)dx}{k\pi\tanh(k\pi H/L)}\cos(k\pi x/L) \\ &\equiv p_0(x,t)+p_1(x,t) \end{aligned} \tag{4.2}$$

The constrained u system is

$$p(x,0,t)+\lambda(t) = mu_{tt}+ru_t+s(x)u-\epsilon u_{xx}, \tag{4.3}$$

$$\int_0^L u(x,t)dx = -AH\omega^{-2}\sin(\omega t+\varphi), \tag{4.4}$$

where we have included a regularizing second-order stiffness term ϵu_{xx}, ϵ being a small, positive constant. The role of this second-order term is to allow us to impose zero Neumann boundary condition on u: $u_x(0,t)=u_x(L,t)=0$, which ensures that $u_{ttx}|_{x=0,L}=0$ so that the series expansion in (4.2) converges uniformly in $x\in[0,L]$. Mechanically, this term adds the longitudinal elastic tension on the membrane,[7] and was considered in BM models[8] earlier.

Now, we truncate the series in (4.2) with its first K terms, and discretize the integral in p_1 by composite trapezoidal rule. The semidiscrete system becomes

$$((mId+4\rho M)(u_{tt})^n)_j-\lambda^n = [p_0-ru_t-su+\epsilon u_{xx}]_j^n, \tag{4.5}$$

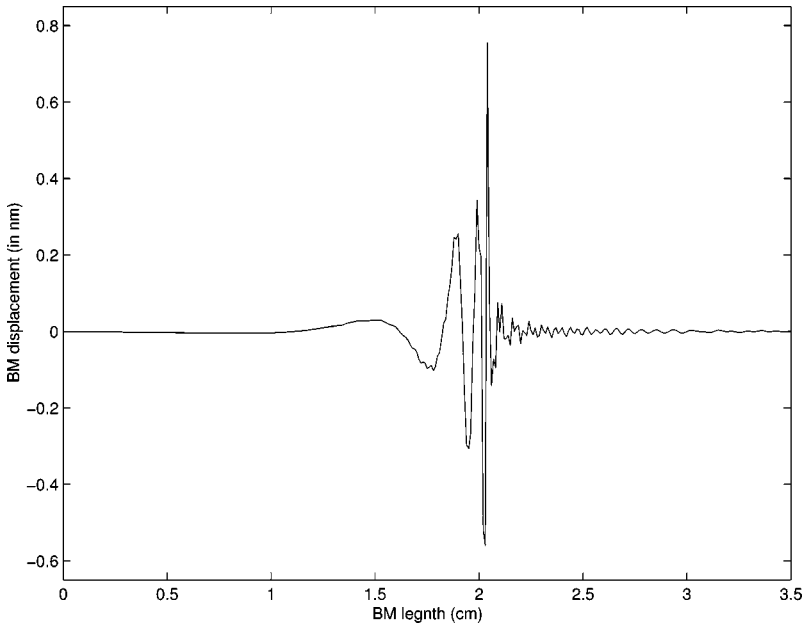

FIG. 3. BM displacement (in nm) at 10 ms with a sinusoidal input of 40 dB (SPL) and 3 kHz, computed by the implicit boundary integral method of the two-dimensional cochlear model with optimal initial data and zero Neumann data on pressure at $x=3.5$ cm. Midear factor is included. Steady state has formed to the left of the characteristic location (about 2 cm), and to the right of it, dispersive instability has been minimized.

where (j,n) denotes the grid points $(x,t)=(j(dx),n(dt))$, dx and dt being spatial and temporal grid steps; Id and M are $J\times J$ matrices; Id the identity, J total number of spatial grid points; $M=(m_{lj})$

$$m_{lj}=hc_j\sum_{k=1}^{K}\frac{\coth(k\pi H/L)}{k\pi}\cdot\cos(k\pi x_l/L)\cdot\cos(k\pi x_j/L),$$

j,l, range between 1 and J; $c_1=c_J=1/2$, $c_j=1$ if $1<j<J$.

Let $Q=\mathrm{diag}(1/2,1,...,1,1/2)$; then, the matrix QM is self-adjoint and non-negative. This is actually a property of the continuum operator from u_{tt} to p_2, which is compact on $L^2([0,L])$ and permits convergent finite dimensional approximations. The need for the diagonal matrix multiplier is due to trapezoidal rule. Hence, the operator $mId+4\rho M$ is invertible as a bounded (spatial) operator uniformly in $K\to\infty$.

The constrained system is further discretized as $(u_{tt})_j^n$ and $(u_t)_j^n$ are replaced by standard second-order central differencing, and

$$(u_{xx})_j^n=\tfrac{1}{4}\delta_x^2(u_j^{n+1}+2u_j^n+u_j^{n-1}),$$

where δ_x^2 is the standard spatial second-order differencing. Such a discretization leads to a stable implicit method so that time step dt is less restricted by dx and steady states are reached in shorter time evolution[4] than by explicit methods. Discretizing the integral in (4.4) by trapezoidal rule, the fully discrete system takes the block form

$$\begin{bmatrix} mId+4\rho M_1 & b_1 \\ b_2^T & 0 \end{bmatrix}\begin{bmatrix} u^{n+1} \\ \lambda^{n+1} \end{bmatrix}=\mathbf{B}(u^n,u^{n-1}), \tag{4.6}$$

where M_1 is symmetrizable by left multiplier Q and QM_1 is positive definite; $b_1=(1,...,1)^T\in R^J$, $b_2=(1/2,1,...,1,1/2)^T$

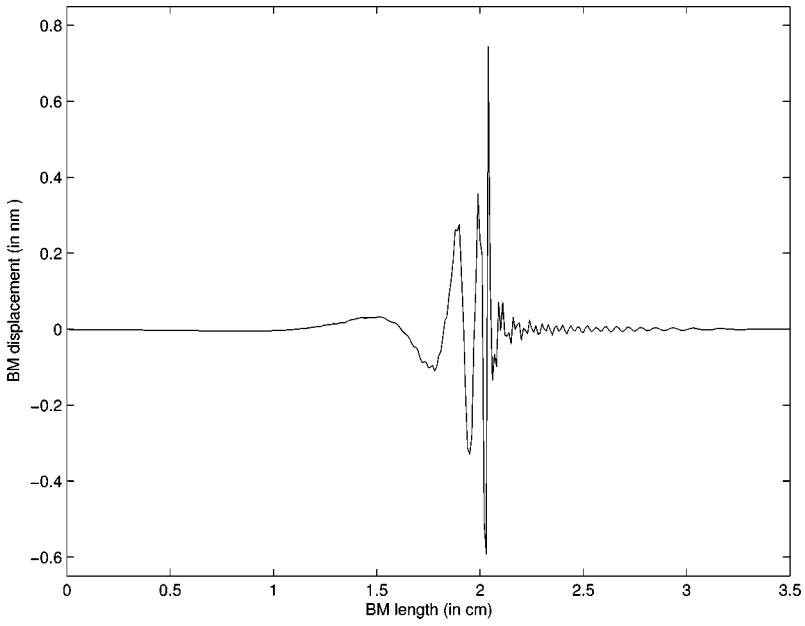

FIG. 4. BM displacement (in nm) at 10 ms with a sinusoidal input of 40 dB (SPL) and 3 kHz, computed by the implicit boundary integral method of the two-dimensional cochlear model with optimal initial data as in (5), and zero Dirichlet data on pressure at $x=3.5$ cm. Midear factor is included. Steady state has formed to the left of the characteristic location (about 2 cm), and to the right of it, dispersive instability has also been minimized by optimal initial data.

$\in R^J$, dots referring to 1's, T the transpose; and vector $\mathbf{B} \in R^{J+1}$ depends only on known values of u at previous time steps. The matrix M_1 is related to M as

$$M_1 = M + (4\rho)^{-1}\left(\frac{dt}{2}\cdot r\cdot Id - \frac{(dt)^2}{4(dx)^2}\cdot \epsilon\cdot M_2\right),$$

and $M_2=(m'_{i,j})$ is the tridiagonal matrix with -2 on the diagonal, and 1 on the off-diagonals, except $m'_{1,2}=m'_{J,J-1}=2$. The vector function $\mathbf{B}$ is:

$$\mathbf{B} = (mId + 4\rho M)(2u^n - u^{n-1}) + \frac{dt}{2} r u^{n-1}$$

$$+ (dt)^2 \frac{\epsilon}{4}\delta_x^2(2u^n + u^{n-1}) - (dt)^2 S u^n + (dt)^2 \mathbf{p}_0^n,$$

where S is the diagonal matrix with $s(j(dx))$'s on the diagonal, $j=1,2,...,J$; $\mathbf{p}_0^n$ has components $p_0(j(dx),n(dt))$, $j=1,2,...,J$. Also, zero Neumann boundary conditions are used when δ_x^2 involves the boundary points.

The block matrix in (4.6) is invertible. In fact, we have the identity

$$\begin{bmatrix} Q & 0 \\ 0 & 1 \end{bmatrix}\begin{bmatrix} mId + 4\rho M_1 & b_1 \\ b_2^T & 0 \end{bmatrix} = \begin{bmatrix} mQ + 4\rho Q M_1 & Qb_1 \\ b_2^T & 0 \end{bmatrix},$$

resulting in a symmetric block matrix of the same form upon noticing that $b_2 = Qb_1$, and Q, QM_1 are symmetric. As b_2 is nonzero and $mQ + 4\rho Q M_1$ is positive definite, the symmetric block matrix is invertible, and so is the block matrix in (4.6).

The method is well-defined with a standard initialization step. For the numerical computation reported here, the initial g function is: $g(x) = 60\max[x^2(1-x)^3, 0]$. The $s(x)$ is a functional fit of the Liberman data[9]

$$s(x) = 4\pi^2 m(0.456\exp(4.83(1-x/3.5)) - 0.45)^2, \tag{4.7}$$

in dyn/cm^3, the mass density $m=0.1$ g/cm^2, the damping constant $r=200$ dyn$\cdot$s/cm^3; the fluid density $\rho=1$ g/cm^3, $L=3.5$ cm, $H=0.1$ cm consistent with parameters in Neely.[5]

The spatial step $dx=0.01$ cm, time step $dt=0.001$ ms, truncation order $K=100$, $\epsilon=10^{-6}$ g/s^2. Smaller ϵ makes no noticeable difference in solutions. The input is a sinusoidal 3-kHz tone of 40 dB SPL, with phase shift $\varphi=0$. At 3 kHz, the midear filter provides a gain factor of about 33, which has been included in the solutions.

Figure 3 shows the computed BM displacement (in nm) at 10 ms with a sinusoidal input of 40 dB (SPL) and 3 kHz. Steady state has formed to the left of the characteristic location (about 2 cm), and to the right of it, dispersive instability has been minimized as our theory predicted. Refined computations and variation of input and model parameters indicate that the optimal initial data work in a robust fashion.

What is striking is that the optimal initial data also minimize the dispersive instability in the case of zero Dirichlet pressure boundary data at $x=3.5$ cm. This is demonstrated in Fig. 4, computed with a similar second-order implicit boundary integral method. Comparing with Fig. 2, we see that the solution captures well the steady-state response. Comparing with Fig. 3, we observe that there is no significant difference between imposing zero Dirichlet or zero Neumann pressure boundary data at $x=3.5$ cm, as in case of the frequency-domain solutions.[5] For this reason, the optimal initial data obtained theoretically from the zero Neumann case apply to the classical model (2.4)–(2.7) as well, though it is not yet clear how to find the exact optimal conditions in the Dirichlet case.

V. CONCLUSIONS

Time-domain computations of steady-state cochlear responses in classical models are subject to dispersive instability. Optimal conditions on initial data are derived and shown to effectively minimize the instability effect for both the zero Neumann and zero Dirichlet pressure boundary conditions at the helicotrema in two-dimensional models. In future work, the analytical conditions on the optimal initial data and the implicit boundary integral method may be extended to time-domain solutions of nonlinear and active cochlear models.[10,11]

ACKNOWLEDGMENTS

This work was supported in part by NSF Grant ITR-0219004, the Faculty Research Assignment Award at the University of Texas at Austin, and a Fellowship from the John Simon Guggenheim Memorial Foundation. I thank M. D. Lamar for preliminary computations, and Y-Y Qi for helpful remarks.

[1] J. B. Allen and M. M. Sondhi, "Cochlear macromechanics: Time domain solutions," J. Acoust. Soc. Am. **66**(1), 123–132 (1979).
[2] R. J. Diependaal, H. Duifhuis, H. W. Hoogstraten, and M. A. Viergever, "Numerical methods for solving one-dimensional cochlear models in the time domain," J. Acoust. Soc. Am. **82**(5), 1655–1666 (1987).
[3] R. J. Diependaal and M. A. Viergever, "Nonlinear and active two-dimensional cochlear models: Time-domain solution," J. Acoust. Soc. Am. **85**(2), 803–812 (1989).
[4] J. Xin, Y-Y. Qi, and L. Deng, "Time domain computation of a nonlinear nonlocal cochlear model with applications to multitone interaction in hearing," Comm. Math Sci. **1**(2), 211–227 (2003). Access on-line at: ⟨www.intlpress.com/CMS/journal⟩
[5] S. T. Neely, "Finite difference solution of a two-dimensional mathematical model of the cochlea," J. Acoust. Soc. Am. **69**(5), 1386–1393 (1981).
[6] M. M. Sondhi, *The Acoustical Inverse Problem for the Cochlea*, Lecture Notes in Biomath Vol. 43, edited by M. Holmes and L. Rubenfeld (Springer, Berlin, 1980), pp. 95–104.
[7] T. Rossing and N. Fletcher, *Vibration and Sound* (Springer, Berlin, 1995).
[8] L. Deng and C. D. Geisler, "Responses of auditory-nerve fibers to multiple-tone complexes," J. Acoust. Soc. Am. **82**(6), 1989–2000 (1987).
[9] M. C. Liberman, "The cochlear frequency map for the cat: Labeling auditory nerve fibers of known characteristic frequency," J. Acoust. Soc. Am. **72**, 1441–1449 (1982).
[10] C. Steele, G. Baker, J. Tolomeo, and D. Zetes, "Cochlear Mechanics," in *Biomedical Engineering Handbook*, edited by J. Bronzino (CRC Press, Boca Raton, FL, 1995), pp. 505–516.
[11] C. Geisler and C. Sang, "A cochlear model using feed-forward outer-hair-cell forces," Hear. Res. **86**, 132–146 (1995).